

## Explosive Nucleosynthesis Associated with Formation of Jet-induced GRBs in Massive Stars

S. Nagataki<sup>1</sup>, A. Mizuta<sup>2</sup>, S. Yamada<sup>3</sup>, H. Takabe<sup>2</sup>, and K. Sato<sup>1,4</sup>

nagataki@utap.phys.s.u-tokyo.ac.jp

### ABSTRACT

We perform 2-dimensional relativistic hydrodynamical simulations in the context of collapsar model. Calculations of explosive nucleosynthesis are also accomplished. We investigate the influence of the structure of the progenitor and energy deposition rate on the resulting explosive nucleosynthesis, assuming that  $^{56}\text{Ni}$  is mainly synthesized in the jet launched by the neutrino heating. We show the amount of  $^{56}\text{Ni}$  is very sensitive to the energy deposition rate. Thus we conclude that it is quite natural not to detect an underlying supernova in some X-ray afterglows as in GRB 010921. We also point out the possibility that the relative abundance of the elements with intermediate mass number such as Si and S in the X-ray afterglow of GRB 011211 may be naturally explained if the energy deposition rate at the central engine is relatively long because little amount of  $^{56}\text{Ni}$  should be synthesized under such an environment. If this discussion is true, there should be correlation between the line features in the X-ray afterglow and duration of the GRB. It should be noted that the duration of GRB 011211 is 270 seconds, making it the longest burst ever observed by Beppo-SAX although it suffers from the effect of red-shift ( $z_{\text{host}} = 2.14$ ), which supports our conclusion. Our results also suggest that the type I collapsar model in which the energy deposition rate is relatively low ( $\dot{E} \sim 10^{51} \text{ erg s}^{-1}$ ) might have difficulty in reproducing the observed amount of  $^{56}\text{Ni}$  in a hypernova such as SN 1998bw. This means that the mechanism of the central engine of a hypernova accompanying GRB may be constrained by the discussion of explosive nucleosynthesis.

---

<sup>1</sup>Department of Physics, School of Science, University of Tokyo, Tokyo 113-0033, Japan

<sup>2</sup>Institute of Laser Engineering (ILE), Osaka University, Yamadaoka, Suita, Osaka 565-0871, Japan

<sup>3</sup>Science and Engineering, Waseda University, Okubo 3-4-1, Shinjyuku, Tokyo 169-8555, Japan

<sup>4</sup>Research Center for the Early Universe, University of Tokyo, Tokyo 113-0033, Japan

*Subject headings:* gamma rays: bursts — supernova: individual: SN 1998bw — nucleosynthesis — hydrodynamics — methods: numerical — relativity

## 1. Introduction

A revolution in our understanding of gamma-ray bursts (hereafter GRBs) occurred in 1997, following accurate localization of GRBs by BeppoSAX (Boella et al. 1997) and the discovery of the afterglow phenomenon. Some GRBs and afterglows are known to have extragalactic origins, which are nicely accounted for by fireball models (Mészáros & Rees 1997), although the origin of the fireball is not yet clear.

However, there has been growing evidence linking GRBs to massive stars. The host galaxies of GRBs are star-forming galaxies and the position of GRBs appear to trace the blue light of young stars (Tsvetkov et al. 2001; Bloom et al. 2002; Floc’h et al. 2003). Some of the host galaxies appear to be dusty with star-formation rates comparable to ultra-luminous infrared galaxies (Berger et al. 2001; Frail et al. 2002). On smaller scales, there is mounting evidence of association with regions of high ambient density (Galama & Wijers 2001; Harrison et al. 2001) and the so-called dark GRBs arise in or behind regions of high extinction (Piro et al. 2002).

Moreover, there has been tantalizing evidence for the existence of an underlying supernova (SN). The first association of a cosmologically distant GRB with the death of a massive star was found for GRB 980326, where a clear excess of emission was observed over and above the rapidly decaying afterglow component. This late-time bump was interpreted as a contribution of an underlying SN (Bloom et al. 1999) since, unlike the afterglow, the bump was very red. GRB 970228, also with an intermediate-time bump and characteristic SN spectral rollover, is another good candidate (Reichart 1999; Galama et al. 2000).

It was also reported that there seems to be a physical connection between GRB 980425 and SN 1998bw (Galama et al. 1998). They discovered an optical transient within the error box of BeppoSAX Wide Field Camera for GRB 980425. It should be noted that this SN is categorized as a new type of SN (i.e. hypernova) with large kinetic energy ( $\sim 10^{52}$  ergs), nickel mass ( $\sim 0.5M_{\odot}$ ), and luminosity (Iwamoto et al. 1998; Woosley et al. 1999). In the analysis of an underlying supernova mentioned above, the light curve of SN1998bw is usually used for the SN template.

Generally speaking, it is considered that it is too difficult to realize a GRB from a death of a massive star, because a fire-ball is required to be composed of enormous radiation energy ( $\sim 10^{51}$  erg) with very small baryon number ( $\sim 10^{-6}M_{\odot}/m_p$ , where  $m_p$

is the proton mass) (Mészáros & Rees 1997). One of the most famous models to realize a GRB and large explosion energy from a death of a massive star is the collapsar model (Woosley 1993; MacFadyen & Woosley 1999). Collapsar is defined as a massive star whose iron core has collapsed to a black hole that is continuing to accrete envelope matter at a very high rate. Woosley also pointed out that there will be two types for collapsars. One (type I collapsar) is that the central core immediately forms a black hole with an accretion disk. In the other case (type II collapsar), the central core forms a neutron star at first, but the neutron star collapses to a black hole with an accretion disk due to the continuous fall back. In both types, it is pointed out that an accretion disk should be formed around the central compact object and neutrinos should be emitted from the innermost region of the accretion disk through the electron (positron) capture and electron-positron pair annihilation (Berezinskii & Prilutskii 1987; MacFadyen & Woosley 1999). Finally, a strong jet with large radiation energy and small baryon number, which is required to produce a GRB, is generated around the polar region due to the pair-annihilation of neutrinos that come from the accretion disk and/or MHD processes. In fact, it is reported that the narrow line of oxygen and broad lines of iron in SN 1998bw can be well reproduced when jet-like explosion is assumed (Maeda et al. 2002).

One may have thought that the system of a GRB has been well known and there is no question about that. That is, a GRB is born from a death of a massive star which collapses and makes a black hole at the center forming a strong jet with a large photon to baryon ratio, large explosion energy of order  $\sim 10^{52}$  ergs, and a great amount of  $^{56}\text{Ni}$  ( $\sim 0.5M_{\odot}$ ) that makes the underlying SN so luminous that it is categorized as a hypernova. However, there are some important problems with GRBs.

First, it is reported that no coincident SN is detected at 99.7% confidence by Hubble Space Telescope in GRB 010921 to a limit 1.34 mag fainter than SN 1998bw. The host galaxy's redshift is relatively low ( $z=0.451$ ), which made intensive multi-color observations possible. It is also pointed out that the observed luminosity of SN 1998bw may be reproduced with a smaller amount of  $^{56}\text{Ni}$  than that required in the spherically-symmetric models by invoking the angle-dependent luminosity expected from asymmetric explosion (Wang et al. 2002). Thus it seems to be still uncertain whether a massive star, that makes a GRB, always produces much of  $^{56}\text{Ni}$ .

Second, there are some reports on the strong iron  $K\alpha$  emission lines (Piro et al. 1998; Piro et al. 2000; Antonelli et al. 2000; Yoshida et al. 2001) in X-ray afterglows. Moreover, there is a report of emission lines of Mg, Si, S, Ar, and Ca with an outflow velocity of order  $0.1c$  in the X-ray afterglow of GRB 011211 (Reeves et al. 2002), although it seems to be still controversial (Rutledge & Sako 2002). At present, the origin of these lines is still open to

arguments. We should investigate whether these features can be explained in the context of collapsar model.

Third, it is an open question whether  $^{56}\text{Ni}$  is synthesized enough to explain the light curve of SN 1998bw in the collapsar model. As explained below, there is an inconsistent treatment between the collapsar model and the hypernova model. In a simulation of the type I collapsar, the mass accretion rate is estimated to be  $\sim 0.07M_{\odot} \text{ s}^{-1}$  in the phase of jet formation (MacFadyen & Woosley 1999), and the timescale of neutrino emission from the accretion disk is also estimated to be about 10 seconds since the temperature of the inner-most region of the accretion disk becomes lower than 1 MeV after that and electron-positron pair creation becomes impossible. As a result, the neutrino emission from the accretion disk ceases (MacFadyen & Woosley 1999; Nagataki et al. 2003). In fact, the thermal energy is usually injected around the polar region at a rate  $\dot{E} \sim 10^{51} \text{ erg s}^{-1}$  for about 10 seconds in numerical simulations, which makes the total explosion energy  $\sim 10^{52}$  ergs (MacFadyen & Woosley 1999; Aloy et al. 2000). On the other hand, in a simulation of explosive nucleosynthesis in the context of a hypernova, total explosion energy is put at once below the mass cut that divides the ejecta from the collapsing core as an initial condition (Maeda et al. 2002). In their simulations, considerable fraction ( $\geq 0.5$ ) of the explosion energy is given as kinetic energy, as opposed to the simulation of collapsars. Also, the progenitor of a hypernova is assumed to be spherical. Thus it should be necessary whether these simulations are consistent with each other or not. That is, we should investigate whether a collapsar model can explain the phenomenon of SN 1998bw as in the hypernova model.

It should be noted here that the accretion disk around the central black hole may be the site where  $^{56}\text{Ni}$  is synthesized (Woosley et al. 1999; MacFadyen & Woosley 1999; Woosley 2002; Pruet et al. 2003). Pruet et al. (2003) calculated electron fractions in the accretion disk and found the proper condition to produce  $^{56}\text{Ni}$  in the disk. They also pointed out the possibility that a considerable amount of  $^{56}\text{Ni}$  can be driven by the disk wind. Although their scenario is widely supported to be very promising, the quantitative evaluation of the yields has yet to be done. In this study, we consider another possibility that  $^{56}\text{Ni}$  is synthesized in the jet, as investigated in Maeda et al. (2002). Thus reader should be reminded that this is our assumption in this study. We also have to note that the opening angle of the jet launched by the neutrino heating has to be large in our scenario, as shown in the following sections, to produce a large enough amount of  $^{56}\text{Ni}$  to explain the luminosity of the hypernova such as SN 1998bw. Such a wide jet will not make a GRB because a bulk Lorentz factor can not be so large as to realize a fireball. Thus, in our scenario, another narrow jet produced possibly by MHD effect or as a small part of the wider jet will be needed to realize a GRB. In this study, however, we do not consider it explicitly, since, if any, it should have little influence on the product of explosive nucleosynthesis because the baryon

mass in the narrow jet should quite small.

In this study, explosive nucleosynthesis is calculated in the context of type I collapsar model. At first, a progenitor collapses and forms a black hole at the center. Next, thermal energy is injected around the polar region to make a jet. Finally, explosive nucleosynthesis is calculated by the post-processing method. We investigate the influence of the progenitor structure and energy deposition rate on the results of explosive nucleosynthesis. We show the amount of  $^{56}\text{Ni}$  is very sensitive to the energy deposition rate. A large amount of  $^{56}\text{Ni}$  is produced when the energy deposition rate is high and vice versa. Thus we conclude that it is quite natural not to detect an underlying SN in some cases. In such cases, we consider that the energy deposition rate was relatively low and a small amount of  $^{56}\text{Ni}$  was synthesized. We also give a discussion on the chemical composition of the ejecta of a collapsar and observed line features in some X-ray afterglows. We point out the possibility that the variation of chemical composition in the X-ray afterglow may be naturally explained by the variation of the energy deposition rate at the central engine. By this discussion, we can predict that there should be correlation between the line features in the X-ray afterglow and duration of the GRB. We also compare the calculated amount of  $^{56}\text{Ni}$  with the observed value in SN 1998bw and investigate which model is best. We show that the type I collapsar model in which the energy deposition rate is relatively low ( $\dot{E} \sim 10^{51} \text{ erg s}^{-1}$ ) may have difficulty in reproducing the observed amount of  $^{56}\text{Ni}$  of SN 1998bw and GRB 980425 and some improvements should be required to explain these observations in the context of the type I collapsar model. This means that the mechanism of the central engine of a hypernova and a GRB is constrained by the discussion of explosive nucleosynthesis.

In section 2, the method of calculation is explained in detail. Results are shown in section 3. Discussions are presented in section 4. Conclusion is given in section 5.

## 2. Method of Calculation

In this section, we present the method of the simulations in this study. It is true that there are some assumptions and simplifications in our simulations. In particular, the effects of gravitation and rotation are not included in this study. In order to realize the jet-induced explosion, we prepare an asymmetric progenitor as an initial condition following the radial infall with the infall timescale depending on the zenith angle. In this way, we can mimic an asymmetric progenitor models of MacFadyen and Woosley (1999). After that, we realize the jet-induced explosion by injecting the thermal energy around the polar region in the same way as MacFadyen and Woosley (1999) did. Of course, this needs improvement in the future. We explain the assumption and simplification in more detail in the following subsections.

## 2.1. Hydrodynamics

### 2.1.1. The Scheme

We performed 2-dimensional hydrodynamic calculations using a spherical coordinate taking account of special relativity. The calculated region corresponds to a quarter of the meridian plane under the assumption of axial-symmetry and equatorial symmetry. The number of mesh points is 500 in the radial direction and 50 in the angular one for the calculation of explosive nucleosynthesis. The radial mesh size is set to be constant in space,  $2 \times 10^7$  cm. With this resolution, the structure of the central accretion disk shown by MacFadyen and Woosley (1999) can be marginally resolved. We did not perform 3-dimensional hydrodynamic calculations simply for saving CPU time and memory. We employed an approximate Riemann solver, Maquina’s flux formula (Donat & Marquina 1996; Donat et al. 1998), for special relativistic hydrodynamic equations. The code is of first order accuracy both spatially and temporally. In this study, we assume that the gas is ideal with the equation of state  $p = \rho\epsilon(\gamma - 1)$ , where  $p$ ,  $\rho$ ,  $\epsilon$ , and  $\gamma$  are pressure, rest mass density, specific internal energy and adiabatic exponent ( $=4/3$  constant in this paper), respectively. Since the hydrodynamics code is Eulerian, we use the test particle method (Nagataki et al. 1997) in order to obtain the informations on the time evolution of the physical quantities along the fluid motion, which are then used for the calculations of the explosive nucleosynthesis. Test particles are scattered in the progenitor and are set at rest at first. They move with the local fluid velocity at their own positions after the passage of the shock wave. The temperature and density that each test particle experiences at each time step are preserved. This is the test particle method we use. See Nagataki et al. (1997) and Nagataki et al. (1998) for more details.

Calculations of hydrodynamics and explosive nucleosynthesis are performed separately, since the entropy produced during the explosive nucleosynthesis is much smaller ( $\sim$  a few%) than that generated by the shock wave. In calculating the total yields of elements, we assume that each test particle has its own mass determined from their initial distribution so that their sum becomes the mass of the layers where these are scattered. It is also assumed that the nucleosynthesis occurs uniformly in each mass element. These assumptions will be justified since the movement of the test particles is not chaotic (i.e. the distribution of test particles at the final time still reflects the given initial condition) and the intervals of test particles are sufficiently narrow to give a smooth distribution of the chemical composition in the ejecta. The number of the test particles are 42000. The test particles are distributed uniformly within the radius of  $7 \times 10^9$  cm.

### 2.1.2. Initial and Boundary Conditions

As for the progenitor of SN 1998bw, it is thought to have had the mass  $\sim 40M_{\odot}$  in the main-sequence stage (Iwamoto et al. 1998; Woosley et al. 1999) and had  $\sim 16M_{\odot}$  helium core (Iwamoto et al. 1998). In this study, the presupernova model obtained from the evolution of  $16 M_{\odot}$  helium core (Nomoto & Hashimoto 1988) is used for the calculation of explosive nucleosynthesis.

As explained above, we make an asymmetric progenitor from the spherical presupernova model by assuming that matter free-falls radially during the times which depend on the zenith angle. The infall time is determined so that the mass of the central black hole becomes  $3M_{\odot}$  at appropriate time and the asymmetric progenitor resembles to the result of MacFadyen and Woosley (1999) in which the effects of gravitation and rotation are taken into account (see their figures 7 and/or 9). The adopted function for the free-fall timescale is

$$t_{\text{fall}} = c_1 \exp(-(\theta/\sigma)^2) \quad [\text{sec}] \quad (1)$$

where  $\theta$  is the zenith angle (in units of radian), and  $c_1$  and  $\sigma$  are set to be 1.0 and  $\pi/4.6$ , respectively. After the radial infall, we can determine the Schwarzschild radius and the baryon mass of the black hole. As mentioned above, the parameters in Eq. (1) are so chosen to give the baryon mass of the central black hole  $3M_{\odot}$ . As will be explained in section 4, the neutrino heating is effective as long as the mass of the central black hole is less than  $\sim 4M_{\odot}$ . Hence, if the mass accretion rate is  $\sim 0.1M_{\odot} \text{ s}^{-1}$  and the duration of the neutrino heating is  $\sim 10 \text{ s}$  as inferred from the result of MacFadyen and Woosley (1999), the mass of the central black hole will be  $\sim 3M_{\odot}$  at the time of the jet launch. In fact, MacFadyen and Woosley (1999) launched the jet when the mass of the central black hole becomes  $3.5M_{\odot}$  in their calculation, which is consistent with our treatment. Aloy et al. (2000) also launched the jet when the mass of the central black hole becomes  $3.762M_{\odot}$  in their calculation. The density, on the other hand, at the innermost region around the polar axis is about  $10^6 \text{ g cm}^{-3}$  and that around the equatorial plane is about  $10^8 \text{ g cm}^{-3}$  in our model, which is similar to the result of MacFadyen and Woosley (1999). This indicates that our prescription Eq. (1) approximately reproduces the more realistic models of MacFadyen and Woosley (1999). It is noted that the accretion disk obtained numerically by MacFadyen and Woosley (1999) well matches the steady state disk (slim disk) model for  $3M_{\odot}$  Schwarzschild black hole (kerr parameter  $a = 0$ ), viscosity parameter  $\alpha = 0.1$ , and accretion rate of  $0.1M_{\odot} \text{ s}^{-1}$  (Popham et al. 1999). Since we here mimiced the numerical result of MacFadyen and Woosley (1999), the situation we consider corresponds to the accretion disk around the black hole with the parameters mentioned above. The dependence of the explosive nucleosynthesis on different initial conditions will be reported in the forth-coming paper. For comparison, we also prepare a spherical model in which the free-fall time does not depend on the zenith

angle. The mass of the central black hole is again set to be  $3M_{\odot}$ . The density contours of the progenitors in this study are shown in Figs. 1 and 2, with the former corresponding to the spherical model and the latter to the asymmetric model. In the asymmetric model, the upper hemisphere is shown.

It will become useful to evaluate the free-fall timescale in the central region of the progenitor and mass accretion rate assuming the free-fall. The free-fall timescale can be estimated as (Woosley 1986)

$$\tau_{\text{ff}} = \frac{1}{\sqrt{24\pi G\rho}} \sim \frac{446}{\rho} \quad [\text{sec}]. \quad (2)$$

The mass accretion rate in the case of free-fall can be also estimated using the mass coordinate and  $\tau_{\text{ff}}$  as

$$\dot{M}(r) = \frac{M_r}{\tau_{\text{ff}}} \quad [M_{\odot} \text{ sec}^{-1}], \quad (3)$$

where  $M_r$  is the mass coordinate which means the enclosed mass within the radius  $r$  from the center of the progenitor. In Fig. 3, we show the estimated free-fall timescale and mass accretion rate in the case of free-fall as a function of the mass coordinate. We can check from the figure that the mass of the central black hole becomes  $\sim 3M_{\odot}$  in 1 second in the case of free-fall. As briefly explained in section 1, the neutrino emission from the accretion disk around the black hole ceases when the temperature of the inner-most region of the accretion disk becomes lower than 1 MeV. This corresponds to the time when the mass of the black hole becomes  $\sim 4M_{\odot}$  (see section 4 and Fig. 12). Thus we can find from the figure that the energy deposition from the accretion disk ceases within 2 seconds in the case of free-fall. Further, we can estimate the thermal energy deposition rate due to the pair annihilation of (anti-)neutrinos as a function of the mass accretion rate, which we will discuss in section 4.

After making the asymmetric progenitor, the thermal energy is injected at the inner-most grid around the polar axis at a rate  $\dot{E} = 10^{51}$  ergs  $\text{s}^{-1}$ , which is a common treatment for the calculations of collapsars (MacFadyen & Woosley 1999; Aloy et al. 2000). We do not consider explicitly how infalling matter are inverted. Instead, we assume that the momentum balance is achieved when the mass of the black hole becomes  $3M_{\odot}$ . After the launch of the jet, the thermal pressure dominates the ram pressure since the accretion energy has declined to about a few times  $10^{50}$  erg  $\text{s}^{-1}$  at that time (MacFadyen & Woosley 1999). For comparison, we also perform the computations in which the total explosion energy ( $= 10^{52}$  ergs) is put instantaneously at the innermost grid around the polar axis. The models investigated in this study are summarized in Table 1. In Models Sa/Aa, the spherical/asymmetric structure is adopted as a progenitor into which thermal energy is injected at a rate  $\dot{E} = 10^{51}$



ergs  $s^{-1}$ . In Models Sb/Ab, the total explosion energy is deposited instantaneously to the spherical/asymmetric structure.

As for the boundary condition, the reflective boundary is adopted on the equatorial plane and symmetry axis for simplicity. It is true that some fraction of explosion energy and matter falls into the black hole. However, we do not observe these energy and matter and are not interested in their chemical composition, either. Hence we consider that the deposited energy in this study corresponds to the observed explosion energy,  $10^{52}$  erg.

## 2.2. Nuclear Reaction Network

Since the chemical composition behind the shock wave is not in nuclear statistical equilibrium, the explosive nucleosynthesis has to be calculated using the time evolution of  $(\rho, T)$  and a nuclear reaction network. We obtain  $(\rho, T)$  comoving with the matter by means of the test particle method mentioned in subsection 2.1.1. The nuclear reaction network contains 250 species (see Table 2). We add some species around  $^{44}\text{Ti}$  to Hashimoto’s network that contains 242 nuclei (Hashimoto et al. 1989), although it turned out that the result was not changed essentially by the addition.

## 3. Results

We first show the results of hydrodynamical calculations. In Figs. 4, 5, and 6, we draw the contours of temperature for the spherical explosion models at  $t = 1.0$  sec, 3.0 sec, and 5.0 sec, respectively. Here we assumed the axial symmetry and equatorial symmetry. The left panel corresponds to Model Sa and the right panel to Model Sb. It is clearly found that the velocity of the shock wave is faster in Model Sb than in Model Sa. This is because the energy density behind the shock is greater in Model Sb, which means that the pressure behind the shock is greater in Model Sb.

In Figs. 7, 8, and 9, we show the contours of temperature for the asymmetric explosion models. In these figures, only the upper hemisphere is shown. The same tendency as in the spherical explosion model, that the velocity of the shock wave is faster in Model Ab than in Aa, is confirmed. It is also clearly shown that the velocity of the shock wave depends on the zenith angle and jetlike explosion is induced, although (as opposed to Maeda et al. 2002) only the thermal energy is injected. This reflects the initial density structure of the progenitor and is consistent with MacFadyen and Woosley (1999).

In Figs. 10 and 11, we show the positions at  $t = 0$  of the test particles with the mass

fraction of  $^{56}\text{Ni}$  greater than 0.3. It is clearly seen that there is almost no region where  $^{56}\text{Ni}$  is synthesized in Models Sa and Aa, whereas  $^{56}\text{Ni}$  is synthesized in large region for Models Sb and Ab. In Table 3, we summarize the abundance of heavy elements in the ejecta for each model, assuming that all unstable nuclei produced in the ejecta decay to the corresponding stable nuclei. The amount of  $^{56}\text{Ni}$  is also shown in the last line. From the table, we can easily confirm that  $^{56}\text{Ni}$ , which decays to  $^{56}\text{Fe}$ , is hardly synthesized in Models Sa and Aa (Note that almost all of  $^{56}\text{Fe}$  is generated from the decay of  $^{56}\text{Ni}$ ). It is emphasized that the amount of  $^{56}\text{Ni}$  synthesized in Models Sa and Aa is less than the required amount to explain the luminosity of SN 1998bw ( $\sim 0.7M_{\odot}$ ; Iwamoto et al. 1998). On the other hand, the amount of  $^{56}\text{Ni}$  synthesized in Models Sb and Ab is almost sufficient to explain the light curve of SN 1998bw. It is noted that the progenitor before the explosion is mainly composed of O, Ne, and Mg (Nomoto & Hashimoto 1988), while the elements heavier than Si are synthesized through the explosive nucleosynthesis (Hashimoto 1995). It is evident in Table 3 that explosive nucleosynthesis occurs and the initial chemical composition of the progenitor is changed to the heavier elements in Models Sb and Ab, while nearly no explosive nucleosynthesis occurs in Models Sa and Aa.

Here we consider why iron elements are hardly synthesized in Models Sa and Aa while much of them are synthesized in Models Sb and Ab. The most significant parameter in explosive nucleosynthesis in a massive star is the temperature. The criterion for the complete silicon burning is  $T_{\text{max}} \geq 5 \times 10^9$  [K] (Thielemann et al. 1996). It is well known that the matter behind the shock wave is radiation dominated and  $T_{\text{max}}$  can be well estimated by equating the supernova (hypernova) energy with the radiation energy inside the radius  $r$  of the shock front

$$E_{\text{HN}} = 10^{52} \left( \frac{E_{\text{HN}}}{10^{52} \text{erg}} \right) = \frac{11\pi^3}{45} \frac{k^4}{\hbar^3 c^3} r^3 T_{\text{max}}^4 \quad [\text{erg}], \quad (4)$$

where  $E_{\text{HN}}$  is the total explosion energy of hypernova,  $k$  is the Boltzmann constant,  $\hbar$  is the Planck constant divided by  $2\pi$ ,  $c$  is the velocity of light. Here a spherical explosion is assumed. This equation gives

$$r = 5.7 \times 10^8 \left( \frac{5 \times 10^9 \text{K}}{T_{\text{max}}} \right)^{4/3} \left( \frac{E_{\text{HN}}}{10^{52} \text{erg}} \right)^{1/3} \quad [\text{cm}]. \quad (5)$$

In the case of Model Sb,  $^{56}\text{Ni}$  is synthesized within the edge for the complete silicon burning ( $\sim 5.7 \times 10^8$  cm). In the case of Model Sa, on the other hand, matter start to move outwards after the passage of the shock wave, and almost all of the matter move away ( $r \geq 6 \times 10^8$  cm) before the injection of all the thermal energy ( $= 10^{52}$  erg). This is the reason why almost no complete silicon burning occurs in Model Sa. The situation should be the same in the asymmetric explosion models. It is apparent from Table 3 that the chemical composition

of the ejecta depends more sensitively on the timescale of thermal energy injection than on the asymmetry of the initial density structure. It should be emphasized that the discussion presented here can also be adopted to the pulsar-powered models for GRBs (Woosley 2002), in which, as Woosley (2002) pointed out, very little nickel will be produced unless a pulsar deposit at least  $10^{51}$  erg in a few tenths of a second. In the next section, we discuss the implication of these results.

#### 4. Discussion

In this study, we assume that  $^{56}\text{Ni}$  is synthesized in the jet as done in Maeda et al. (2002). In this section, we give further discussion under this assumption.

First, as stated in section 1, it is reported that no coincident SN is detected in GRB 010921 to a limit of 1.34 mag fainter than SN 1998bw at 99.7% confidence is detected by Hubble Space Telescope. If we simply interpret this result as a lack of  $^{56}\text{Ni}$  in GRB 010921, the amount of  $^{56}\text{Ni}$  synthesized in GRB 010921 is less than  $0.7M_{\odot}/(2.512^{1.34})\sim 0.2M_{\odot}$ , which can be naturally explained by Models Sa and Aa. We want to emphasize that the amount of  $^{56}\text{Ni}$  in the ejecta can be small even if the total explosion energy is much larger than that of the normal collapse-driven supernova, as long as the energy deposition rate is relatively low. We insist that observations like GRB 010921 can be naturally explained in the context of the type I collapsar model.

Second, we discuss the features of line emission in some X-ray afterglows. As stated in section 1, strong iron  $K\alpha$  emission lines are found in X-ray afterglows (Piro et al. 1998; Piro et al. 2000; Antonelli et al. 2000; Yoshida et al. 2001). There is also a report of emission lines of Mg, Si, S, Ar, and Ca with an outflow velocity of order  $0.1c$  in the X-ray afterglow of GRB 011211 (Reeves et al. 2002). According to Reeves et al. (2002), the relative abundance of the light metals (Mg, Si, S, Ar, Ca) was found to be  $\sim 9$  times the solar value, whereas the relative abundance of iron was found to be  $\leq 1.4$  times the solar value. Although the mechanism of such emission lines is still controversial (Paczýński 1998; Lazzati et al. 1999; Rees & Mészáros; Vietri et al. 2001; Kotake & Nagataki 2001; Kosenko et al. 2002), we want to point out that the chemical composition in the X-ray afterglow may be naturally explained if the effects of the energy deposition rate are taken into account, as shown in this study. Here the origin of the emission lines is assumed to be the ejecta from the underlying SN (HN). One may think that the relative abundance of iron becomes small when the effect of fallback is taken into account. However, if the jetlike explosion occurs to generate a GRB, iron elements are synthesized around the jet axis as shown in Fig. 11. In this case, it will be hard to consider that the relative abundance of iron becomes small due to the effects of the

fallback. According to Reeves et al. (2002), the velocity of the outflow which emits the lines of heavy elements is of order  $0.1c$ , which is about ten times faster than the velocity of the ejecta in the normal collapse-driven supernova (Nagataki et al. 1998; Nagataki 2000). The required kinetic energy is easily estimated as

$$E_{\text{kin}} = 9 \times 10^{51} \left( \frac{M}{1M_{\odot}} \right) \left( \frac{v}{0.1c} \right)^2 \text{ erg}, \quad (6)$$

which means that the underlying SN is a hypernova. We emphasize again that the abundance of the elements with intermediate mass number such as Si and S becomes greater than that of iron even if a hypernova explosion is adopted as long as the timescale of the energy deposition is long. If this discussion is true, there should be correlation between the chemical composition of the ejecta and the timescale of the energy deposition. This should mean that there should be correlation between the line features in the X-ray afterglow and the duration of the GRB. If the emission lines are mainly composed of light elements such as Si and S, the duration of the GRB should be relatively long and vice versa. In fact, it is reported that the duration of GRB 011211 is 270 seconds, making it the longest burst ever observed by Beppo-SAX (Reeves et al. 2002). Although the interpretation of the line feature of X-ray afterglow of GRB 011211 seems to be still controversial (Rutledge & Sako 2002), we hope the increase of observations in near future.

Third, we consider that the observations of SN 1998bw can be well explained by Models Sb and/or Ab, but not by Models Sa and Aa. This means that the energy deposition timescale should be relatively short ( $\ll 10$  sec) in order to explain the luminosity of SN 1998bw by the type I collapsar model. One may think that the amounts of  $^{56}\text{Ni}$  produced in Models Sb and Ab ( $0.14M_{\odot}$  and  $0.16M_{\odot}$ , respectively) are still less than the observed value ( $\sim 0.7M_{\odot}$ ; Iwamoto et al. 1998). However, the total explosion energy is assumed to be  $\sim 3 \times 10^{52}$  ergs in Iwamoto et al. (1998) while it is decreased to  $10^{52}$  ergs in this study. Thus, we consider that the observed amount can be explained with no problem when the total explosion energy is set to be  $\sim 3 \times 10^{52}$  ergs in Models Sb and/or Ab. If we believe the conclusion derived by Maeda et al. (2002) that the line features in SN 1998bw can be well reproduced by the jet-induced explosion model, Model Ab seems to be the best one. However, we argue below that it seems to be difficult even for the models Sb and Ab to generate a GRB. At present, we are led to the conclusion that there seems to be no model to generate a GRB associated with a hypernova synthesizing much iron.

Now we discuss whether the results obtained in this study can constrain the model of the central engine of a hypernova accompanied by a GRB. According to the scenario of the type I collapsar model, the explosion energy larger than that of the normal collapse-driven supernova may be given by the pair annihilation of neutrinos from the accretion

disk around the central black hole. It takes about several seconds from the beginning of the core collapse to form an accretion disk. In the meantime, the matter around the polar region falls directly into the central black hole. This is because the matter around the polar region possess smaller angular momentum. As a result, the polar region may become an adequate environment for generating a fireball. The timescale to form a fireball is determined by the timescale of neutrino emission from the accretion disk, which is about 10 seconds (MacFadyen & Woosley 1999). Although we pointed out in this study that the type I collapsar model can naturally explain the observations of GRB 010921 and GRB 011211 in which little amount of iron is required, this scenario may face difficulty in producing a large amount of  $^{56}\text{Ni}$  required in SN 1998bw, since the energy deposition rate is too low. If the energy deposition timescale is forced to be shorter ( $\ll 10$  sec), it seems to become doubtful whether a GRB can be really generated, as explained below. To make the energy deposition rate greater means the larger the mass accretion rate. This corresponds to the case in which the total angular momentum in the central region of the progenitor is small. Then, it is doubted that whether an asymmetric explosion occurs and an adequate environment for generating a fireball is achieved around the polar region. That is, we suspect that the density around the polar region can not become low enough to realize a fireball when the mass accretion around the equatorial plane is large. This is because there is little time for the mass around the polar region to fall into the black hole before the explosion due to the pair annihilation of neutrinos occurs.

Let us investigate the above discussion quantitatively. Popham et al. (1999) proposed an accretion-disk model including the effect of general relativity as a collapsar model (Popham et al. 1999). This model and the numerically computed collapsar model (MacFadyen & Woosley 1999) are reproduced well by the analytical model of the accretion disk by Nagataki et al. (2002). The density, the temperature and the disk thickness are fitted as follows (see Nagataki et al. 2002 for details).

$$\rho [\text{g cm}^{-3}] = 8.23 \times 10^8 \left(\frac{M}{3M_{\odot}}\right)^{-1.7} \left(\frac{\dot{M}}{0.1M_{\odot}\text{s}^{-1}}\right)^{1.03} \frac{1}{\left(\frac{r}{r_s}\right)^{1.07} \left(1 + \left(\frac{r}{r_s}\right)\right)^{0.76}}, \quad (7)$$

$$T [\text{MeV}] = 2.3 \times \left(\frac{M}{3M_{\odot}}\right)^{-0.2} \left(\frac{\dot{M}}{0.1M_{\odot}\text{s}^{-1}}\right)^{0.108} \frac{1}{\left(\frac{r}{r_s}\right)^{0.425} \left(1 + \left(\frac{r}{r_s}\right)\right)^{0.21}}, \quad (8)$$

$$H [\text{cm}] = 5.8 \times 10^6 \left(\frac{M}{3M_{\odot}}\right)^{0.9} \left(\frac{\dot{M}}{0.1M_{\odot}\text{s}^{-1}}\right)^{-0.0183} \frac{1}{\left(\frac{r}{r_s}\right)^{-1.66} \left(1 + \left(\frac{r}{r_s}\right)\right)^{0.3867}}, \quad (9)$$

where  $M$  is the mass of the central black hole,  $r$  is the radial coordinate, and  $r_s$  ( $= 10^7\text{cm}$ ) is the core radius, respectively. Note that the Schwarzschild radius is  $\simeq 8.862\text{km}(M/3M_\odot)$ . We see from Eq. (8) that as the mass of the central black hole grows, the temperature becomes lower, and the flux of neutrinos decreases. In Fig. 12, we show the duration of neutrino emission. This (almost) corresponds to the timescale in which the temperature at the innermost region of the accretion disk becomes lower than  $\sim 1$  MeV. This will approximately reflect the timescale of GRB. In this figure the initial mass of the central black hole was set to be  $3M_\odot$ . The time when the temperature of the inner-most region of the accretion disk becomes lower than 1 MeV almost corresponds to the time when the mass of the black hole becomes  $\sim 4M_\odot$ . From this figure, we find that the mass accretion rate has to be larger than several  $M_\odot \text{ s}^{-1}$  so that the energy deposition timescale is shorter than 1 second. This mass accretion timescale is shorter than that presented in MacFadyen and Woosley (1999). On the other hand, if the mass accretion is so rapid, there will be no time to make an adequate environment to produce a fireball around the polar region as mentioned above. Of course, we can not conclude that the type I collapsar model is ruled out by the discussion of the explosive nucleosynthesis as a model of hypernova associated with GRB. We guess that there will be some ways to solve the difficulty presented in this study. However, we believe that it is very important to point out that the central engine of a GRB accompanied by SN (HN) explosion can be constrained by the discussion of the explosive nucleosynthesis. At present, we have to say that the Type I collapsar model is required to be improved so as to explain the observed luminosity in SN 1998bw. It is noted that MacFadyen and Woosley (1999) pointed out the possibility that a substantial amount of  $^{56}\text{Ni}$  is produced in the accretion disk and a part of it is conveyed outwards by the viscosity-driven wind (see their figure 16; see also (Pruet et al. 2003)). Their scenario will be important and it should be investigated whether the behavior of the light curve and the line features of iron and oxygen can be explained in such a framework as well as the jetlike explosion model (Maeda et al. 2002). In the study of Maeda et al. (2002), the narrow line of oxygen and broad lines of iron can be explained when a jet-induced explosion is assumed.

We consider that the variation of the energy deposition rate is naturally caused by the variation of the progenitor's initial angular momentum. Thus it may be still too early to consider that a GRB is always accompanied by a hypernova that generates a large amount of iron elements. This is what we want to stress in this paper and we expect the increase of observations in near future.

As mentioned in section 1, the accretion disk around the central black hole may be the site of  $^{56}\text{Ni}$  synthesis (Pruet et al. 2003). This scenario is widely supported to be most promising, although the quantitative evaluation of the yield is remaining to be done. If true, there may not be any correlation between the duration of GRB and the amount of

synthesized  $^{56}\text{Ni}$  (the collapsar without the disk wind may make too little  $^{56}\text{Ni}$  in any case). Thus it might be possible to distinguish two scenarios by future observations.

In this study, we used the nuclear reaction network which contains 250 species (see table 2). Thus we could not discuss the nucleosynthesis of heavier elements such as in the r-process nucleosynthesis. We consider that the polar region within the jet may be an adequate site for r-process nucleosynthesis (MacFadyen & Woosley 1999; Nagataki 2000; Nagataki 2001). We are planning in near future to perform the calculation of r-process nucleosynthesis in the context of jetlike explosion presented in this study.

In this study, we modeled the jet launched by the neutrino heating and a large opening angle of the jet was necessary for the jet to produce a large enough amount of  $^{56}\text{Ni}$  to explain the luminosity of the hypernova such as SN 1998bw. As stated in section 1, such a wide jet will not make a GRB because a bulk Lorentz factor can not be sufficiently large to realize a fireball. Therefore, to realize a GRB in our scenario, another narrow jet might be needed supposedly launched by MHD effect. If the jet is launched by the MHD effect (Blandford & Znajek 1977), a considerable fraction of the explosion energy should be in the form of kinetic energy and/or magnetic field energy (Zhang et al. 2003). As a result the temperature should be lower compared with the neutrino heating model until the reverse shock converts the kinetic energy into the thermal energy (Zhang et al. 2003). Thus the explosive nucleosynthesis will be unlikely to occur in this scenario unless the reverse shock propagates inwards immediately and makes the temperature high enough to cause the explosive nucleosynthesis.

We made in this study an asymmetric initial progenitor model by a simple prescription. This treatment should be, of course, improved. We are planning to perform numerical calculations of core collapse in a massive star that leads to a black hole formation including the effects of gravity, rotation and neutrino transfer (Yamada & Sato 1994; Yamada 1997; Kotake et al. 2003). We will then investigate in detail the dependence of explosive nucleosynthesis on the density structure at the time of the jet launch as a function of initial angular momentum in a progenitor based on their results in the near future.

## 5. Conclusion

We have performed numerical calculations of explosive nucleosynthesis in the context of the collapsar model using 2D relativistic hydrodynamical simulations. We have investigated the influence of the structure of the progenitor and energy deposition rate on the explosive nucleosynthesis, assuming that  $^{56}\text{Ni}$  is mainly synthesized in the jet. We have shown the

amount of  $^{56}\text{Ni}$  is very sensitive to the energy deposition rate rather than the structure of the progenitor. We conclude that it is quite natural to detect no underlying SN in some cases, such as GRB 010921. We have pointed out that the relative abundance of the elements with intermediate mass number such as Si and S in the X-ray afterglow of GRB 011211 is naturally explained if the energy deposition rate at the central engine is relatively small. We also predicted that there should be correlation between the line features in the X-ray afterglow and the duration of the GRB. Interestingly, the duration of GRB 011211 is 270 seconds, the longest burst ever observed by Beppo-SAX although it suffers from the effect of red-shift ( $z_{\text{host}} = 2.14$ ). Our results also imply that the type I collapsar model in which the energy deposition rate is relatively low ( $\dot{E} \sim 10^{51} \text{ erg s}^{-1}$ ) as shown in MacFadyen and Woosley (1999), may have difficulty in reproducing the observed amount of  $^{56}\text{Ni}$  in SN 1998bw. This means that the mechanism of the central engine of hypernova and GRB is constrained by the discussion of explosive nucleosynthesis. We hope that the increase of observations will lead to the improvement of theories on GRB in near future.

The authors thank to Dr. Blinnikov for useful comments. S.N. thanks the Yukawa Institute for Theoretical Physics at Kyoto University, where this work was initiated during the YITP-W-01-06 on 'GRB2001' and completed during the YITP-W-99-99 on 'Blackholes, Gravitational Lens, and Gamma-Ray Bursts'. Hydrodynamic calculations were carried out on NEC SX-5 system at Cybermedia Center, Osaka University. This research has been supported in part by the Grant-in-Aid by the Ministry of Education, Culture, Sports, Science and Technology of Japan (No.14079202, No.S14102004, No.S14740166).

## REFERENCES

- Aloy, M.A., et al., 2000, ApJ, 531, L119
- Antonelli, L.A., et al. 2000, Science, 290, 953
- Berezinskii, V.S., & Prilutskii, O.F., 1987, A&A, 175, 309
- Berger, E., et al. 2001, ApJ, 556, 556
- Blandford, R.D., & Znajek, R.L., 1977, MNRAS, 179, 433
- Bloom, J.S., et al. 1999, Nature, 401, 453
- Bloom, J.S., Kulkarni, S.R., & Djorgovski, S.G. 2002, AJ, 123, 1111
- Boella, G., et al., 1997, A&AS, 122, 299



- Donat, R., & Marquina, 1996, *J. Comp. Phys.*, 125, 42
- Donat, R., Font, J. A., Ibáñez, J. M<sup>a</sup>., & Marquina, 1998, *J. Comp. Phys.*, 146, 58
- Floc'h, E.Le, et al. 2003, *A&A*, 400, 499
- Frail, D.A., et al., 2002, *ApJ*, 565, 829
- Galama, T.J., et al., 1998, *Nature*, 395, 670
- Galama, T.J., et al. 2000, *ApJ*, 536, 185
- Galama, T.J., & Wijers, R.A.M.J., 2001, *ApJ*, 549, L209
- Harrison, F.A., et al. 2001, *ApJ*, 559, 123
- Hashimoto, M., Nomoto, K., Shigeyama, T. 1989, *A&A*, 210, L5
- Hashimoto, M., 1995, *Prog. Theor. Phys.*, 94, 663
- Iwamoto, K., et al., 1998, *Nature*, 395, 672
- Kotake, K., & Nagataki, S., 2001, *PASJ*, 53, 579
- Kotake, K., Yamada, S., & Sato, K., 2003, *ApJ*, in preparation.
- Kosenko, D.I., Blinnikov, S.I., Postnov, K.A., Lundqvist, P., & Sorokina, E.I., 2002, *astro-ph/0211382*
- Lazzati, D., Campana, S., & Ghisellini, G., 1999, *astro-ph/9902058*
- MacFadyen, A.I., Woosley, S.E., *ApJ*, 1999, 524, 262
- MacFadyen, A.I., 2003, *astro-ph/0301425*
- Maeda, K., et al., 2002, *ApJ*, 565, 405
- Mészáros, P.M., & Rees, M.J., 1997, *ApJ*, 476, 232
- Nagataki, S., Hashimoto, M., Sato, K., & Yamada, S. 1997, *ApJ*, 486, 1026
- Nagataki, S., Shimizu, T.M., & Sato, K. 1998, *ApJ*, 495, 413
- Nagataki, S., 2000, *ApJS*, 127, 141
- Nagataki, S., 2001, *ApJ*, 551, 429

- Nagataki, S. et al., 2003, *APh*, 18, 551
- Nomoto, K., & Hashimoto, M. 1988, *Phys. Rep.*, 163, 13
- Paczyński, B., 1998, *ApJ*, 494, L45
- Piro, L., Amati, L., & Antonelli, L.A., 1998, *A&A*, 331, L41
- Piro, L., et al., 2000, *Science*, 290, 955
- Piro, L., et al., 2002, *ApJ* (in press), astro-ph/0201282
- Popham, R., Woosley, S.E., & Fryer, C., 1999, *ApJ*, 518, 356
- Pruet, J., Woosley, S.E., & Hoffman, R.D., 2003, *ApJ*, 586, 1254
- Rees, M.J., & Mészáros, P.M., 2000, astro-ph/0010258
- Reeves, J.N., et al., 2002, astro-ph/0206480
- Reichart, D.E., 1999, *ApJ*, 521, L111
- Rutledge, R.E., & Sako, M., 2002, astro-ph/020673
- Thielemann, F.-K., Nomoto, K., & Hashimoto, M., 1996, *ApJ*, 460, 408
- Tsvetkov, D.Y., Blinnikov, S.I., & Pavlyuk, N.N. *Astronomy Letters*, 2001, 27, 411
- Vietri, M., Ghisellini, G., & Lazzati, D., 2001, astro-ph/0011580
- Wang, L., et al., astro-ph/0206386
- Woosley, S.E., 1986, in *Nucleosynthesis and Chemical Evolutions*, eds. B. Hauck, A. Maeder, G. Meynet (Geneva: Geneva Observatory), 1
- Woosley, S.E., *ApJ*, 1993, 405, 273
- Woosley, S.E., Eastman, R.G., & Schmidt, B.P., 1999, *ApJ*, 516, 788
- Woosley, S.E., astro-ph/0211063
- Yamada. S., & Sato. K., 1994, *ApJ*, 434, 268
- Yamada, S., 1997, *ApJ*, 475, 720
- Yoshida, A., et al., 2001, *ApJ*, 557, L27

Zhang, W., Woosley, S.E., & MacFadyen A.I., 2003, ApJ, 586, 356

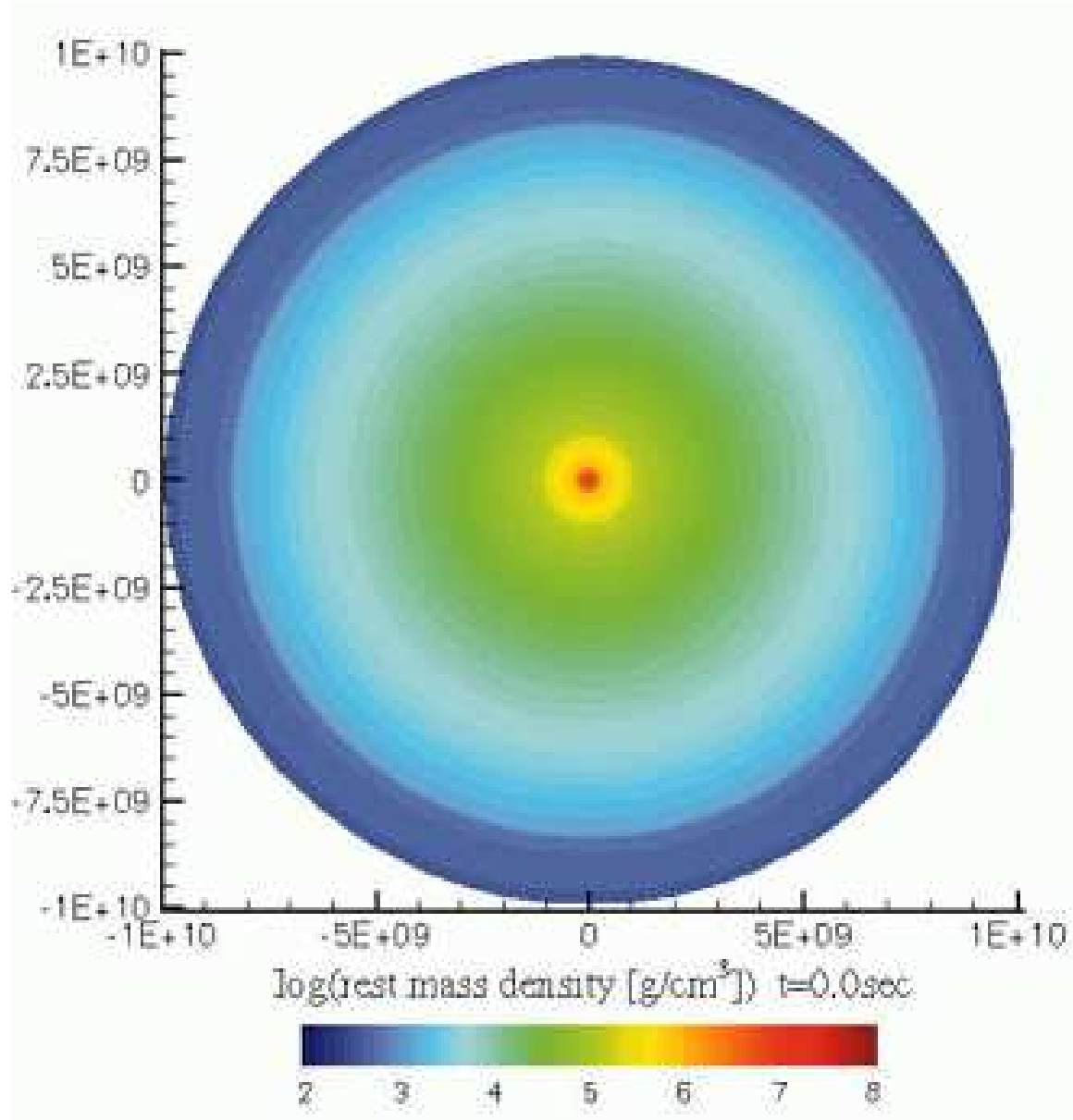


Fig. 1.— Initial density contour for the spherical model. The free-fall time is determined so that the mass of the central black hole becomes  $3M_{\odot}$ .

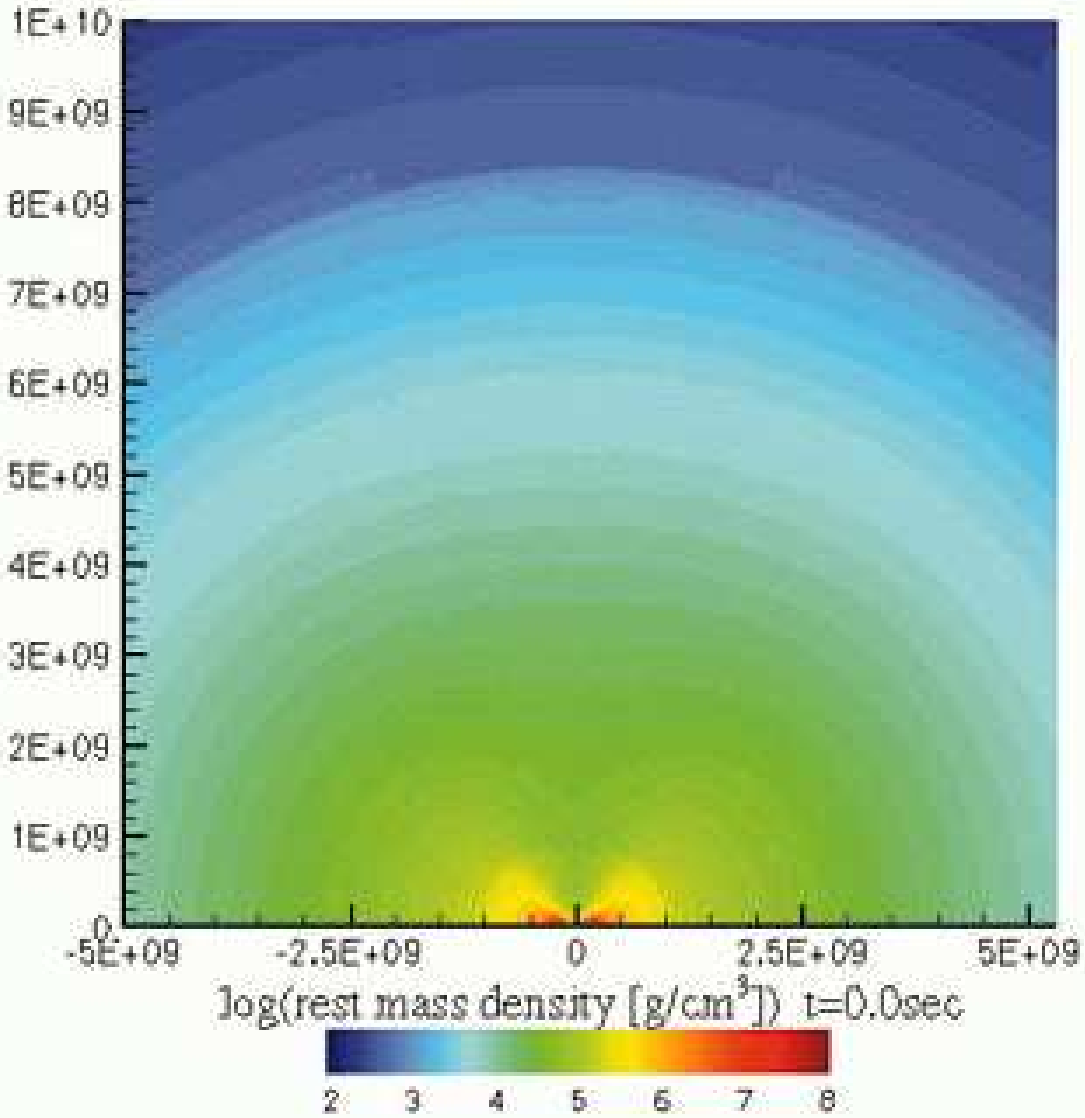


Fig. 2.— Same as Fig.1 but for the asymmetric model and only the northern hemisphere is shown. The asymmetric model is made by allowing only the radial infall and assuming that the infall timescale depends on the zenith angle. The infall time is determined so that the central mass of the black hole becomes  $3M_{\odot}$  and the density structure resembles to the result of MacFadyen and Woosley (1999).

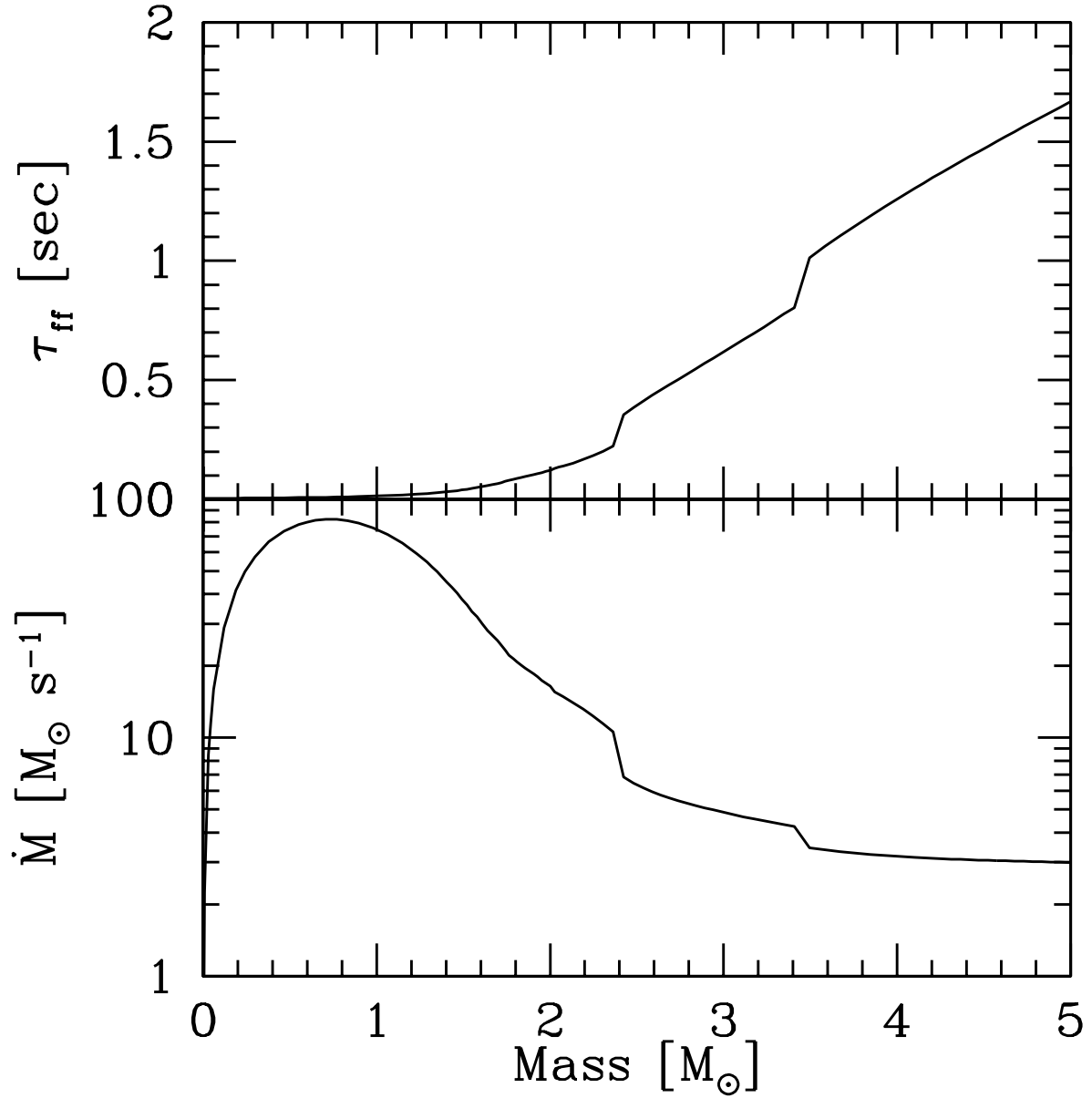


Fig. 3.— Upper: free-fall timescale as a function of the mass coordinate. Lower: mass accretion rate in the case of free-fall.

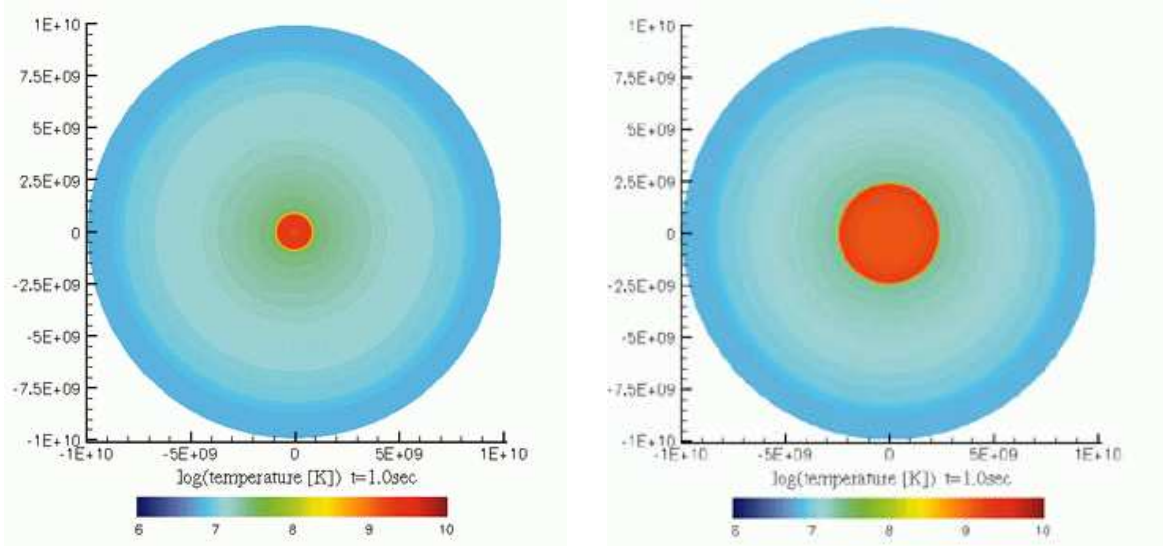


Fig. 4.— Contours of temperature at  $t = 1.0$  sec. Left panel corresponds to Model Sa and right panel corresponds to Model Sb.

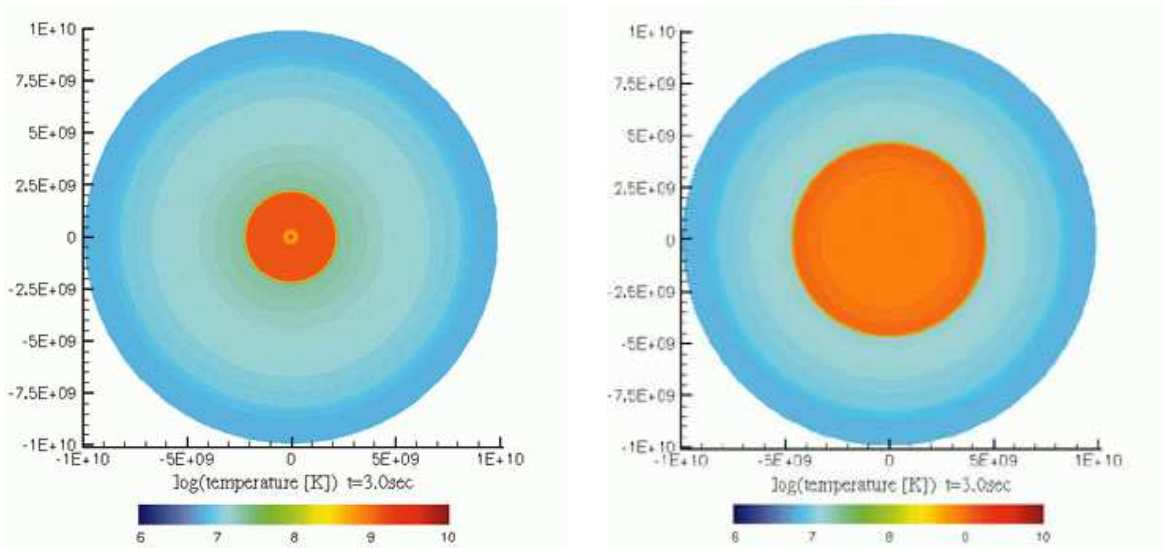


Fig. 5.— Same as Fig.4, but for  $t = 3.0$  sec.

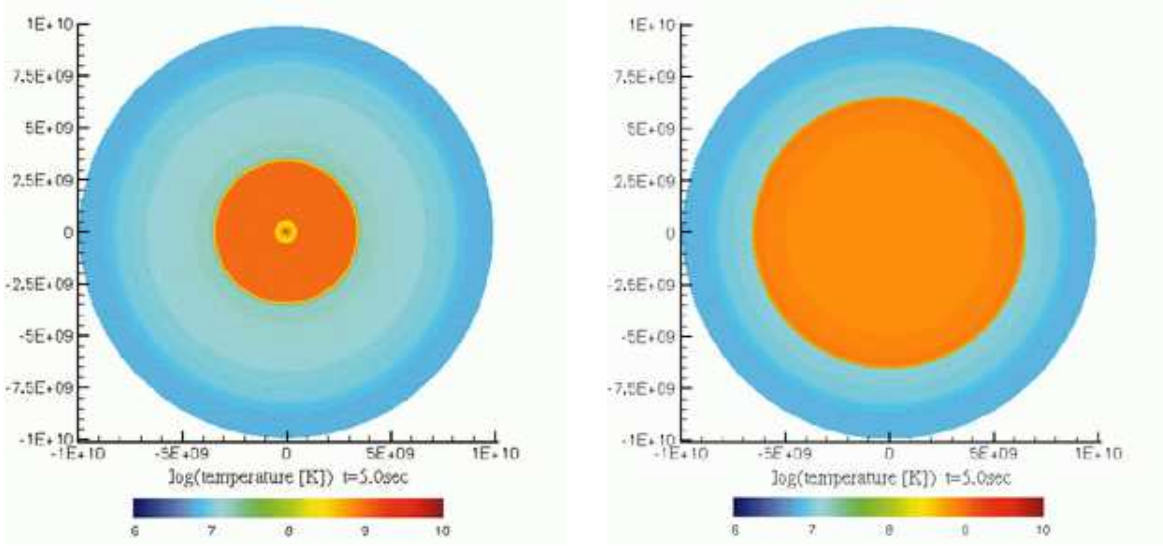


Fig. 6.— Same as Fig.4, but for  $t = 5.0$  sec.

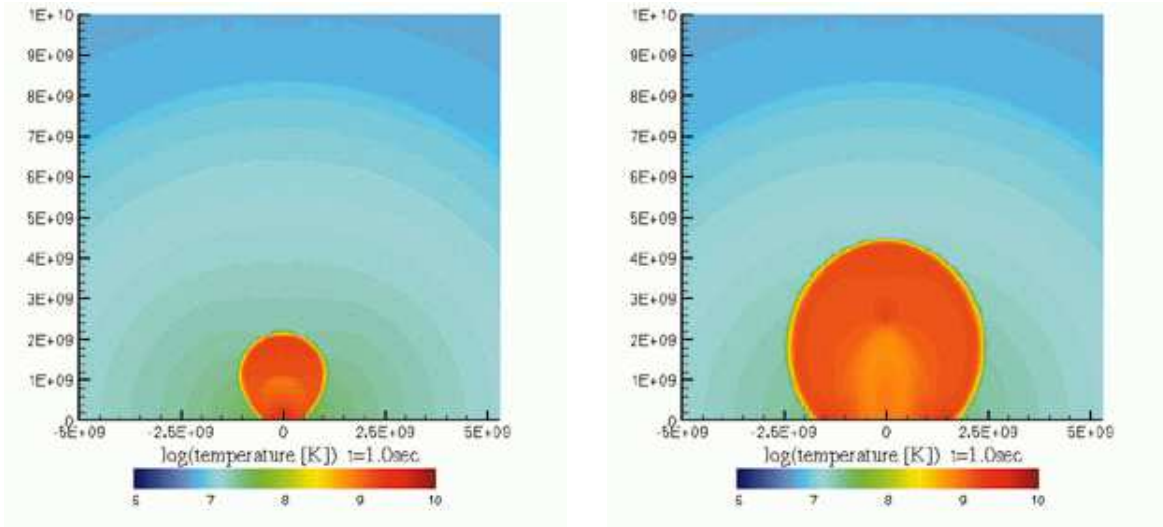


Fig. 7.— Contours of temperature at  $t = 1.0$  sec. Left pannel corresponds to Model Aa and right pannel corresponds to Model Ab. Only the northern heimsphere is shown.



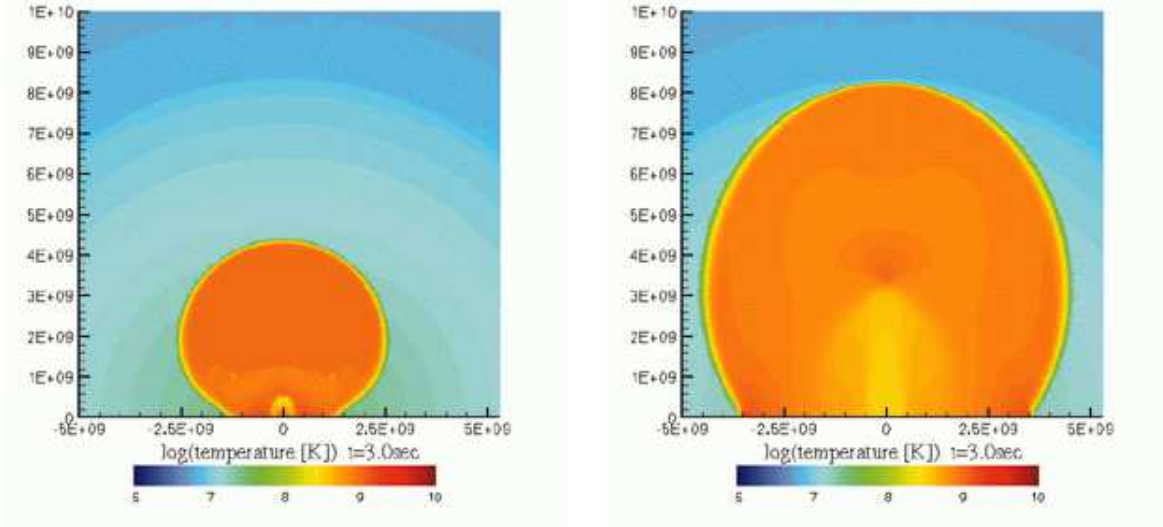


Fig. 8.— Same as Fig.7, but for  $t = 3.0$  sec.

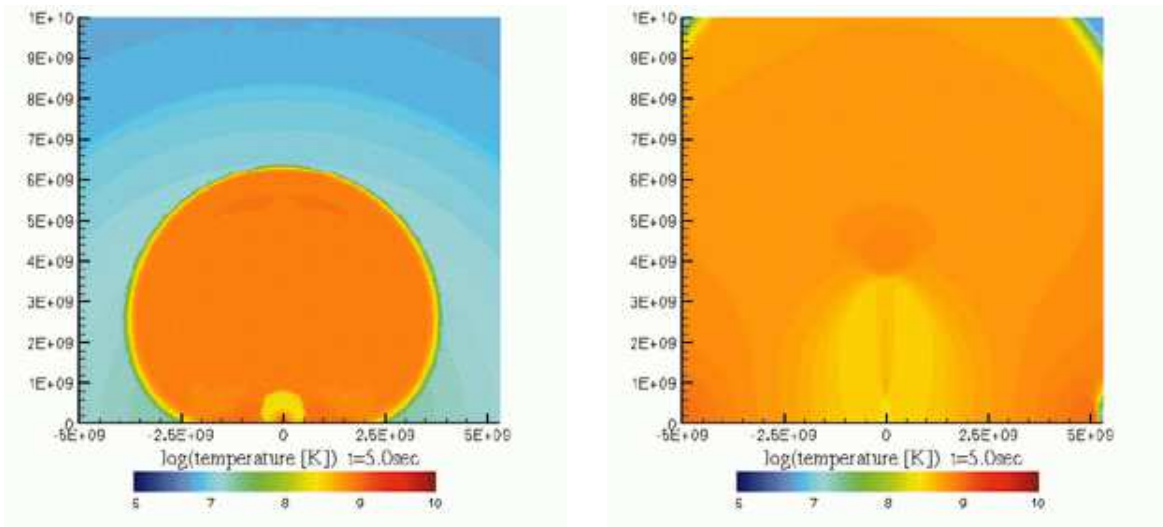


Fig. 9.— Same as Fig.7, but for  $t = 5.0$  sec.

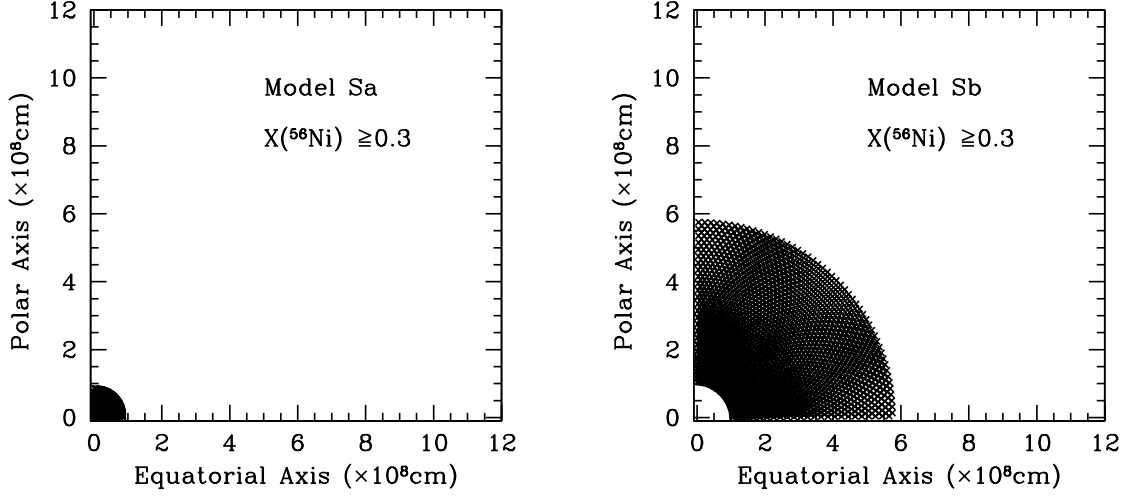


Fig. 10.— Positions of the test particles at  $t = 0$  sec that meet the condition that the mass fraction of  $^{56}\text{Ni}$  becomes greater than 0.3. Left panel corresponds to Model Sa whereas right panel corresponds to Model Sb.

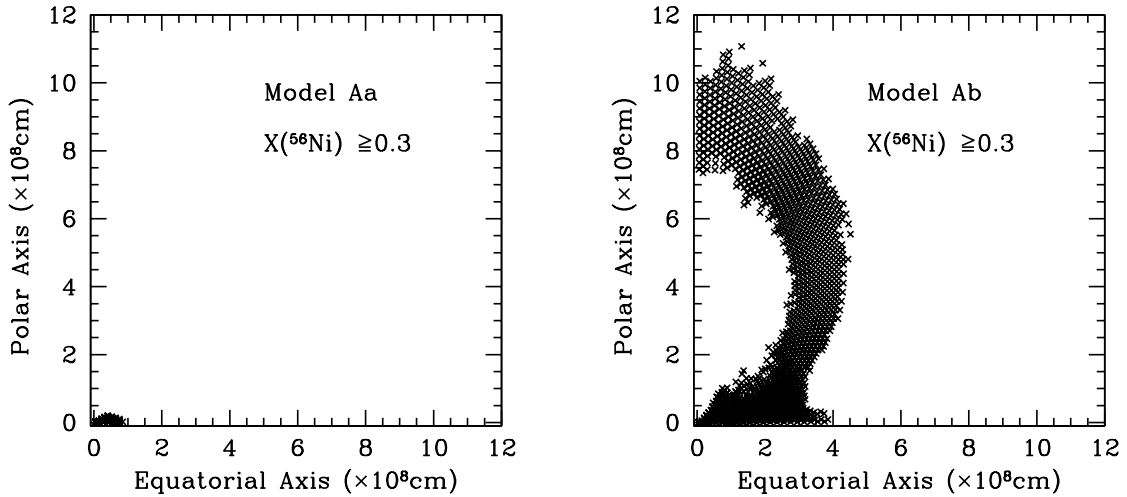


Fig. 11.— Same with Fig.10 but for the asymmetric models. Left panel corresponds to Model Aa whereas right panel corresponds to Model Ab.

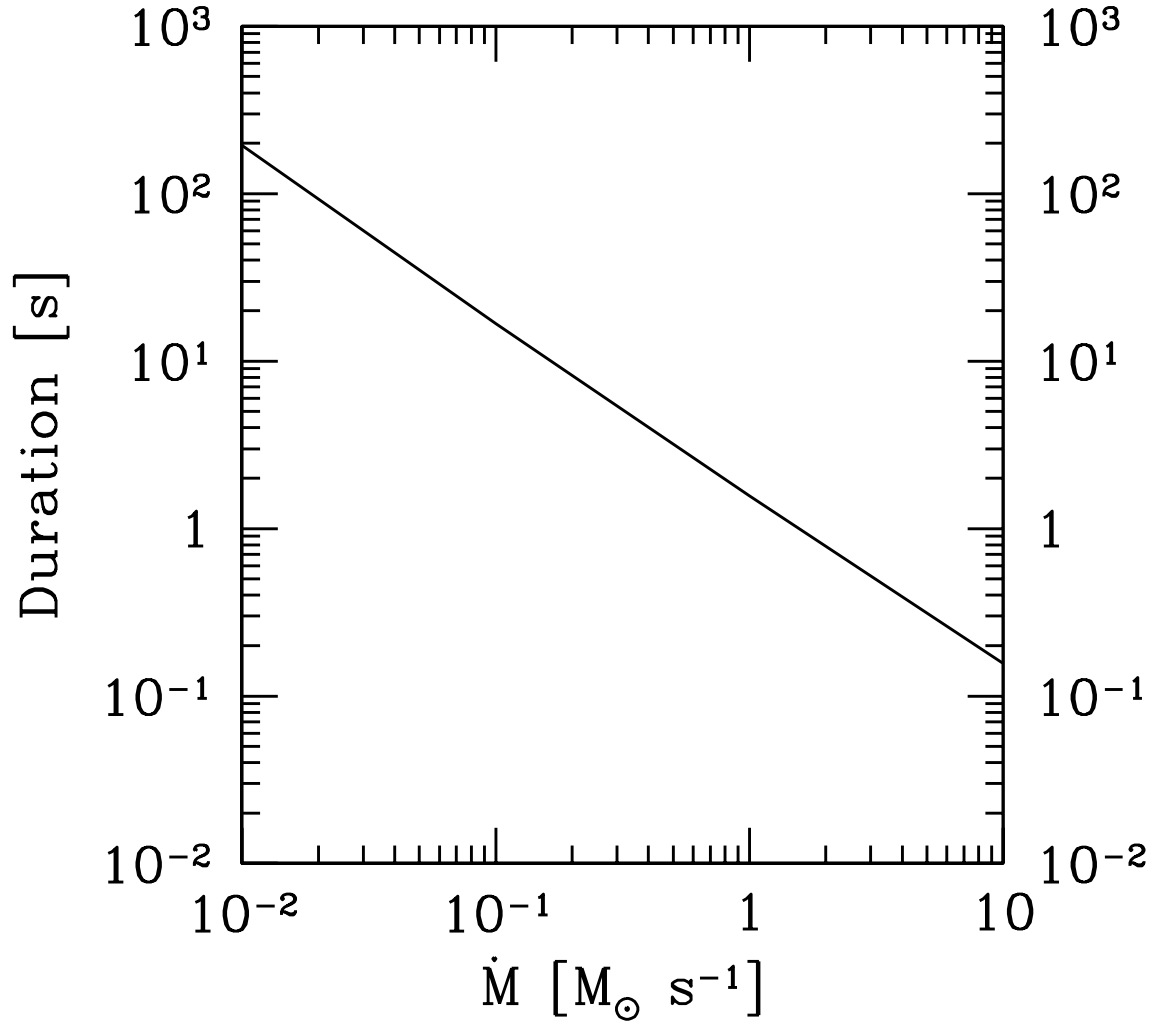


Fig. 12.— Duration of the neutrino emission from a collapsar as function of the mass-accretion rate. The initial mass of the central black hole is set to be  $3M_{\odot}$ .

Model	progenitor	$\dot{E}$ [erg s <sup>-1</sup> ]	$E_{\text{tot}}$ [erg]
Sa	spherical	10 <sup>51</sup>	10 <sup>52</sup>
Sb	spherical	$\infty$	10 <sup>52</sup>
Aa	asymmetric	10 <sup>51</sup>	10 <sup>52</sup>
Ab	asymmetric	$\infty$	10 <sup>52</sup>

Table 1: Models, structure of the progenitor, thermal energy deposition rate (erg s<sup>-1</sup>), and total explosion energy. See detail in section 2.1.2.

Element	A <sub>min</sub>	A <sub>max</sub>	Element	A <sub>min</sub>	A <sub>max</sub>	Element	A <sub>min</sub>	A <sub>max</sub>
N	1	1	Al	24	30	V	44	54
H	1	1	Si	26	33	Cr	46	55
He	4	4	P	28	36	Mn	48	58
C	11	14	S	31	37	Fe	52	61
N	12	15	Cl	32	40	Co	54	64
O	14	19	Ar	35	45	Ni	56	65
F	17	22	K	36	48	Cu	58	68
Ne	18	23	Ca	39	49	Zn	60	71
Na	20	26	Sc	40	51	Ga	62	73
Mg	22	27	Ti	42	52	Ge	64	74

Table 2: Nuclear Reaction Network Employed

Element	Model Sa	Model Sb	Model Aa	Model Ab
O	9.3E+0	8.8E+0	9.1E+0	8.5E+0
Mg	5.4E-1	5.0E-1	5.3E-1	4.9E-1
Si	2.4E-1	3.8E-1	2.4E-1	3.1E-1
S	3.3E-2	1.2E-1	3.4E-2	9.0E-2
Ar	6.6E-3	2.4E-2	7.7E-3	1.8E-2
Ca	4.5E-3	1.9E-2	5.6E-3	1.7E-2
Ti	1.2E-5	9.4E-4	8.3E-6	1.0E-3
Fe	1.4E-2	3.1E-1	8.0E-2	3.7E-1
<sup>56</sup> Ni	6.1E-3	1.4E-1	2.7E-2	1.6E-1

Table 3: Abundance of heavy elements in the ejecta for each model in units of  $M_{\odot}$ . All unstable nuclei produced in the ejecta are assumed to decay to the corresponding stable nuclei. The amount of <sup>56</sup>Ni is also shown in the last row.